

# MaTe: Images Are All You Need for Material Transfer via Diffusion Transformer

Nisha Huang<sup>1,2</sup>, Henglin Liu<sup>1</sup>, Yizhou Lin<sup>1</sup>, Kaer Huang<sup>3</sup>, Chubin Chen<sup>1</sup>,  
Jie Guo<sup>2,†</sup>, Tong-Yee Lee<sup>4</sup>, Xiu Li<sup>1,†</sup>

<sup>1</sup>Tsinghua University, <sup>2</sup>PengCheng Laboratory, <sup>3</sup>Lenovo Research, <sup>4</sup>National Cheng-Kung University

<sup>1</sup>{hns24, liu-hl24, yz-lin24, chenb24}@mails.tsinghua.edu.cn, li.xiu@sz.tsinghua.edu.cn

<sup>2</sup>{huangnsh, guoj01}@pcl.ac.cn <sup>3</sup>huangke1@lenovo.com <sup>4</sup>tonylee@mail.ncku.edu.tw



Figure 1. **MaTe** is a material transfer method that enables the transformation of textures from a single real-world image without any prior knowledge. This approach is not only capable of successfully extracting texture information from antiques with thousands of years of history but also handles popular computer graphics images, jewelry, and fur materials, providing strong support for design work.

## Abstract

Recent diffusion-based methods for material transfer rely on image fine-tuning or complex architectures with assistive networks, but face challenges including text dependency, extra computational costs, and feature misalignment. To address these limitations, we propose *MaTe*, a streamlined diffusion framework that eliminates textual guidance and reference networks. *MaTe* integrates input images at the token level, enabling unified processing via multi-modal attention in a shared latent space. This design removes the need for additional adapters, *ControlNet*, inversion sampling, or model fine-tuning. Extensive experiments demonstrate that *MaTe* achieves high-quality material generation under a zero-shot, training-free paradigm. It outperforms state-of-the-art methods in both visual quality and efficiency while preserving precise detail alignment, significantly sim-

plifying inference prerequisites.

## 1. Introduction

Material transfer is a technique that precisely maps the properties of a specific material sample onto the surface of a target object, as shown in Fig. 1. Due to its broad application prospects in digital content creation and industrial design, this technology has garnered attention in recent years. Traditional material transfer frameworks primarily rely on parametric modeling paradigms, such as optical reflection models based on bidirectional scattering distribution function (BRDF) [5, 10, 14] or procedural texture generation algorithms [13, 44]. These frameworks limit the diversity of the generated results due to the limited size of the basic material library, failing to meet the customization needed for non-uniform composite materials in digital artistic creation.

In recent years, inspired by the breakthroughs of diffusion models in conditional generation tasks, diffusion-based material transfer methods [27, 38, 42] have achieved remarkable improvements in high-quality material transfer effects. Current state-of-the-art (SOTA) approaches often employ fine-tuning of diffusion models with sample sets bound to text identifiers [37, 42, 49] (in Fig. 2 (a)), implicitly encoding material features through conceptual semantic binding. Although these methods address some shortcomings of traditional pipelines, their heavy reliance on text prompts restricts fine-grained control of material properties. Moreover, the full-parameter fine-tuning paradigm significantly increases training costs and the risk of overfitting. The latest studies [3, 9] have also introduced pre-trained general image encoders IP-Adapters [43] to extract material features, as well as ControlNet [47] to inject depth information, as shown in Fig. 2 (b). However, these methods frequently induce hierarchical decoupling between material and structural information (instead of seamless fusion) during generation, while also suffering from prolonged inference times.

To address the limitations of prior works, we revisit the necessity of employing additional image encoders in material transfer tasks, aligning with cutting-edge trends in image generation research [4, 7, 24, 28]. The core objective of material transfer lies in ensuring consistent alignment of texture attributes on the target object’s surface with the visual details of the material exemplar. When multiple independent conditional control signals are injected in parallel without cross-modal interaction mechanisms, they often induce inter-modal decoupling phenomena. This manifests as isolated encoding of material features, geometric structures, and illumination information in the latent space, where each modality independently influences the generation process rather than enabling feature fusion through collaborative optimization. Such limitations typically result in artifacts like material-geometry misalignment, where material textures fail to conform to surface curvature, and illumination-reflection inconsistency, where specular highlights deviate from light source directions.

The above insights, combined with the emergence of the Diffusion Transformer (DiT) paradigm [31], motivate us to re-examine fundamental approaches for material transfer. Although IP-Adapter and ControlNet effectively represent material and structural information individually, limitations such as inconsistent feature spaces, lack of interaction modules, and information competition during generation hinder the natural fusion of material, depth, and input images in diffusion models (in Fig. 4 (d)-(g)). We consider that semantic alignment across multimodal features and their interactive potential within a shared latent space should be prioritized, thus projecting all image conditions into a unified latent representation. We design a novel MaTe architecture that processes image conditions in a unified

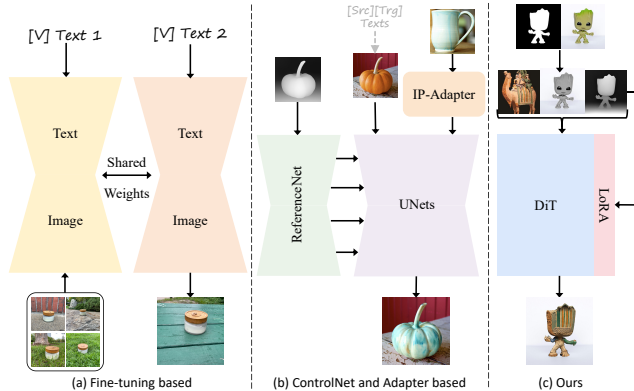


Figure 2. Simplified structure comparison of different kinds of material transfer methods. Our approach neither relies on fine-tuning image sets/individual images nor requires additional image encoding by IP-Adapters. It only requires basic image information as input, rather than complex text guidance, to obtain high-quality material transfer results.

manner through multimodal attention, eliminating reliance on complex control modules. The Unified-Sequence Processing and Cross-Bias Modulation mechanisms in MaTe enable the denoising network to jointly handle all image signals, requiring only lightweight Low-Rank Adaptation (LoRA) [12] to augment depth information.

In summary, we highlight our contributions as follows:

- We propose MaTe, a concise material transfer architecture that enables semantic interaction between image conditions alongside zero-shot control, significantly reducing architectural complexity and inference time.
- We simplify the inference process, eliminating the need for fine-tuning or manually setting text information. We achieve the inference of all necessary information from input images using existing pre-trained diffusion models.
- We construct a diverse and extensive real-world material transfer evaluation dataset. Our method produces high-quality material transfer results with consistent details, outperforming SOTA baselines in both qualitative and quantitative analyses.

## 2. Related work

### 2.1. Image-guided generation.

Image-guided generation is a challenging yet promising field, leveraging visual guidance for content creation. The emergence of diffusion models [15, 16, 31, 36] has significantly propelled advancements in this field, enabling SOTA performance across a wide range of generative visual tasks, such as image-to-image translation [17, 18, 43], subject-driven image generation [11, 37], etc. DreamBooth [37] and Textual Inversion [8] leverage transfer learning for text-to-image (T2I) diffusion models to enable customized concept generation via full parameter fine-tuning or word vector op-

timization. To enhance the controllability of image-guided generation, adapter-based architectures have emerged as bridges between external control signals (e.g., sketches) and diffusion models. ControlNet [47] first validates an adapter that can be trained to capture task-specific input conditions, while T2I-adapter [29] employs a lightweight adapter to achieve fine-grained control in the color and structure of the generated images. IP-Adapter [43] allows for more flexible and intuitive control of the generation process, expanding the capabilities of image-guided generation. These methods demonstrate image-conditioned generation strategies with varying specificity, suggesting potential pathways for addressing material transfer challenges.

## 2.2. Material acquisition and transfer.

Material acquisition and transfer represent a realm of research considering illumination conditions, object geometry, and physical properties of materials. Traditional 3D material transfer methods, such as Text2tex [1], TEXTure [35], and TextureDreamer [45], rely on 3D geometric shapes and lighting estimation, followed by careful adjustment of material properties. As a result, the quality and diversity are restricted, presenting limited and unsatisfactory results. In contrast, 2D-to-2D material transfer, bypassing ground-truth 3D data, is challenging yet highly practical. Prevalent approaches based on fine-tuning including DreamBooth [37], Material Palette [27], Prospect [49] and U-VAP [42] fine-tune diffusion models on small sample sets associated with text identifiers. While existing methods mitigate conventional pipeline limitations, text prompts reliance restricts control and fine-tuning risks computational costs, and overfitting. Another category of methods, such as MaterialFusion [9] and ZeST [3], uses extra encoder modules like IP-Adapter [43] or ControlNet [47] to extract material features. When multiple image conditions are injected into the network in parallel, the material and structure information in the results are separated into two independent layers, lacking semantic integration (see Fig. 4 (d)-(g)). The latest SOTA method MaterialFusion [9] applies DDIM inversion [39] to both the material and the input images, which increases the sampling steps and time by more than double. Different from methods that rely on text-assisted fine-tuning or complex architectures with additional reference networks, our method MaTe projects material, content, and depth images into the same latent space and performs semantically aligned generation.

## 3. Method

MaTe is a training-free, non-text prompts, and zero-shot image-to-image framework with structure and material control. Given the target image  $I_{\text{input}}$  and the material image  $I_M$ , MaTe produces an output image  $I_o$  that inherits the structure from  $I_{\text{input}}$  and the material from  $I_M$ . Our ap-

proach is illustrated in Fig. 3 and summarized as follows: After providing the target image  $I_{\text{input}}$  and the material image  $I_M$ , in Sec. 3.3, we obtain the illumination image  $I$  and the depth image  $I_D$ .  $I_M$ ,  $I$ , and  $I_D$  undergo *Unified-Sequence Processing* and *Cross-Bias Modulation* through our designed MaTe architecture to achieve control over structure and material. Additionally, LoRA is used to enhance the depth effect, and *Background-Preserving Blending* is employed to strengthen the consistency of the foreground and background through Sec. 3.3.

### 3.1. Preliminary

**Rectified-Flow Models.** Generative models aim to define a mapping from samples  $x_1$  from a noise distribution  $p_1$  to samples  $x_0$  from a data distribution  $p_0$ , where  $p_0$  represents real images in image generation tasks. Rectified flows [25, 26] define a forward process that constructs paths between distributions  $p_0$  and  $p_1$  as straight trajectories, as shown in Eq. 1, where  $p_1 = \mathcal{N}(0, 1)$ . Here, the forward process is time-dependent due to timestep  $t$ .

$$x_t = (1 - t)x_0 + t\epsilon, \quad \epsilon \sim N(0, 1) \quad (1)$$

To learn this mapping, a network is trained with parameters  $\theta$ , to estimate the velocity  $v$  of the rectified flow, represented by  $v_\theta$ . By adopting the reparameterization from [7], this velocity prediction network can serve as a noise prediction network,  $\epsilon_\theta$ , optimized using the Conditional Flow Matching (CFM) objective formulated as Eq. 2.

$$\mathcal{L}_{CFM} = -\frac{1}{2} \mathbb{E}_{t \sim \mathcal{U}(t), \epsilon \sim \mathcal{N}(0, I)} [w_t \lambda'_t \|\epsilon_\theta(x_t, t) - \epsilon\|^2] \quad (2)$$

Here,  $\lambda'_t$  represents the re-parametrized signal-to-noise ratio, and  $w_t$  is a time-dependent weighting function.

**Multi-Modal Diffusion Transformers.** The DiT model [31], is employed in architectures like FLUX.1 [21], Stable Diffusion 3 [7], and PixArt [2] use transformer as denoising network to refine noise image tokens iteratively. As shown in Fig. 3 (a), the DiT model processes two token types: noise image tokens  $X \in \mathbb{R}^{N \times d}$  and text condition tokens  $C_T \in \mathbb{R}^{M \times d}$ , where  $d$  is the embedding dimension,  $N$  and  $M$  are the number of image and text tokens respectively. Throughout the network, these tokens maintain consistent shapes as they pass through multiple transformer blocks. In FLUX.1, each DiT block consists of layer normalization followed by multi-modal attention (MMA) [30], which incorporates rotary position embedding (RoPE) [40] to encode spatial information.

The multi-modal attention mechanism then projects the position-encoded tokens into query  $Q$ , key  $K$ , and value  $V$  representations. It enables the computation of attention between all tokens:

$$\text{MMA}([X; C_T]) = \text{softmax} \left( \frac{QK^\top}{\sqrt{d}} \right) V, \quad (3)$$

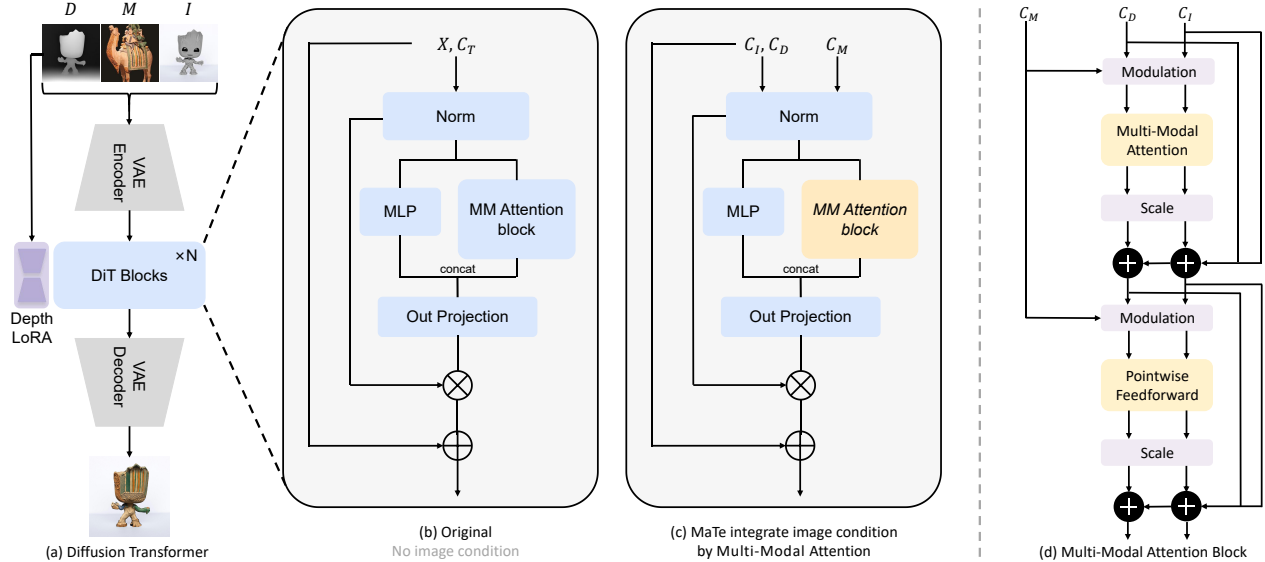


Figure 3. Our method achieves high-quality material transfer by simply passing three types of image tokens (material image tokens  $C_M$ , depth image tokens  $C_D$ , and illumination image tokens  $C_I$ ) through the multimodal attention mechanism of DiT for interaction, ensuring that they remain in the same feature space throughout the diffusion process. It eliminates the need for unnecessary image fine-tuning and text guidance, resulting in a streamlined inference process.

where  $[X; C_T]$  denotes the concatenation of image and text tokens. This formulation enables bidirectional attention. Building on the DiT architecture with FLUX.1 as the implementation basis, we aim to develop MaTe, a framework that balances superior performance with minimalist design, guiding material transfer exclusively via visual conditions.

### 3.2. Depth and Illumination Guidance

**Lighting Consistency.** Diffusion models typically start sampling from random noise, which can lead to the lighting loss of optical priors in the initial image. As ZeST [3], we adopt a foreground grayscale image  $I$  to retain illumination without base color prior. The denoising process is initialized using the following formula:

$$I = F \odot I_{gray} + (1 - F) \odot I_{input} \quad (4)$$

Here,  $F$  denotes the object mask, and  $I_{gray}$  represents the grayscale image. This formula achieves the decoupling of lighting preservation and material interference: The component  $(1-F) \odot I_{input}$  retains the environmental lighting characteristics (direction, intensity, and hue), while  $F \odot I_{gray}$  eliminates the inherent base color contamination of the source object while maintaining geometric shadow information. As shown in the ablation study in Fig. 7, the illumination image  $I$  can better preserve the illumination information compared to random noise.

**Geometric Guidance Optimization.** Given the inherent challenges in decoupling geometric and material attributes within images and the requirement for additional training data, we propose an enhanced solution that integrates depth image  $D$  as geometric priors within the diffusion

model, reinforcing the structural representation of target objects through a lightweight standard way. Comparative experiments (detailed in Sec. 4.5) demonstrate our rejection of conventional ControlNet architectures (e.g., [23] with 1.59B parameters) in favor of a FLUX.1 depth-aware LoRA module [12] (620M parameters). Experimental validation confirms this design achieves a 1.8 speedup in inference for material transfer tasks while maintaining geometric fidelity.

### 3.3. MaTe

**Architecture Designing.** To achieve both versatility architectural changes, MaTe first reuses the VAE encoder [20, 36] from the base DiT, treating the illumination image  $I$  as the noise image and projecting the material image into the same latent space as the noise image tokens. This approach contrasts sharply with previous methods that rely on separate feature extractors (e.g., IP-Adapter [3, 9, 43]), significantly reducing architectural complexity. We achieve material transfer by leveraging the spatial correspondence in the multi-modal attention block, without the need for targeting specific subjects. The encoded depth condition tokens  $C_D$  share the same dimensionality and latent space as the illumination image tokens  $C_I$ , enabling them to be directly processed by the Transformer blocks. Since both condition and image tokens reside in the same latent space, MaTe leverages the existing DiT blocks to jointly process them. Notably, we innovatively propose *Cross-Bias Modulation*, a novel mechanism that enables controllable cross-modal interaction through structured logarithmic bias, thereby achieving free control among conditions.

**Low-Rank Adaptation.** The LoRA approach enhances pa-

parameter efficiency by freezing the pre-trained weight matrices and introducing additional trainable low-rank matrices within the neural network. This method is based on the observation that pre-trained models exhibit low “intrinsic dimension”. Specifically, for a weight matrix  $W \in \mathbb{R}^{n \times m}$  in the diffusion model  $\epsilon_\theta$ , incorporating a LoRA module involves updating  $W$  to  $W'$ , defined as  $W' = W + BA$ . Here,  $B \in \mathbb{R}^{n \times r}$  and  $A \in \mathbb{R}^{r \times m}$  are matrices of a low-rank factor  $r$ , satisfying  $r \ll \min(n, m)$ . In our work, we employ a LoRA module to control depth information [22]. By assigning a specific weight  $w$  to the LoRA module, we can modulate its influence on the generation process:

$$W' = W + w \times BA. \quad (5)$$

The weight  $w$  is typically a hyperparameter determined through empirical tuning and is used to balance the relationship between depth information and other generative features. This allows LoRA to effectively incorporate depth information into the diffusion model to produce images that conform to the depth structure, unlike previous material transfer methods that use ControlNet.

**Unified-Sequence Processing.** Previous methods, such as ControlNet [47] and T2I-Adapter [29], introduced condition images into the model through direct feature addition:

$$X \leftarrow X + C_D, \quad (6)$$

where the condition features  $C_D$  are spatially aligned and added to the noise image tokens  $X$ . While this method is effective for spatially aligned tasks, it faces two limitations: (1) it lacks flexibility in non-aligned scenarios where spatial correspondence does not exist, and (2) the rigid addition operation constrains potential interactions between condition and image tokens. In contrast, MaTe directly concatenates condition tokens with the image tokens  $[C_M; C_I; C_D]$  for multi-modal attention processing. This new operation enables flexible token interactions through DiT’s multi-modal attention mechanism, allowing direct relationships to emerge between any pair of tokens without imposing strict spatial constraints.

**Cross-Bias Modulation.** While MaTe’s unified sequence processing and multi-modal attention enable effective token interactions during training, practical applications often require adjustable conditioning strength at test time. We achieve this by introducing a bias term into the multi-modal attention computation. Specifically, for a given strength factor  $\gamma$ , we modify the attention operation in Equation 3 to:

$$\text{MMA}([C_M; C_I; C_D]) = \text{softmax} \left( \frac{QK^\top}{\sqrt{d}} + B(\gamma) \right) V, \quad (7)$$

where  $B(\gamma)$  is a bias matrix modulating the attention between concatenated tokens  $[C_M; C_I; C_D]$ . Given  $C_M \in$

$\mathbb{R}^{M \times d}$  and  $C_I, C_D \in \mathbb{R}^{N \times d}$ , the bias matrix has the structure:

$$B(\gamma) = \begin{bmatrix} \mathbf{0}_{M \times M} & \log(\gamma) \mathbf{1}_{M \times N} & \log(\gamma) \mathbf{1}_{M \times N} \\ \log(\gamma) \mathbf{1}_{N \times M} & \mathbf{0}_{N \times N} & \mathbf{0}_{N \times N} \\ \log(\gamma) \mathbf{1}_{N \times M} & \mathbf{0}_{N \times N} & \mathbf{0}_{N \times N} \end{bmatrix}. \quad (8)$$

The bias matrix structure ensures that the attention patterns within each modality (main diagonal blocks) remain unchanged, while the interaction strength between modalities ( $C_M$  and  $C_I/C_D$ ) is modulated by introducing a  $\log(\gamma)$  bias term. During the testing phase, when  $\gamma \rightarrow 0^+$  (taking an extremely small value), the influence of the condition can be eliminated, and when  $\gamma > 1$ , the condition guidance is enhanced by increasing the cross-modal attention weights. This method allows for flexible control over the integration strength of image conditions and generation results without the need to retrain the model.

**Background-Preserving Blending.** A simple method for preserving the background is to replace the generated background with the original one, taken from the input image:  $x' \odot m + x \odot (1 - m)$ . The obvious issue is that combining the two images in this way fails to produce a coherent, seamless result. Our key hypothesis is that at each step of the diffusion process, a noise latent representation is projected onto a manifold of natural images that are noised to a certain level. While blending two noise images (from the same level) may yield a result that likely lies outside the manifold, the next diffusion step projects the result onto the next level manifold, thereby ameliorating the incoherence.

Therefore, at each stage, starting from the latent representation  $x_t$ , a diffusion step is performed according to the conditional prompt, yielding a latent representation denoted as  $x_{\text{gen}}$ . This is combined with the noise version of the original input image  $x_{\text{in}}$  obtained from the input image. The two latent representations are now blended using the mask:

$$x_{t-1} = x_{t-1, \text{gen}} \odot m + x_{t-1, \text{in}} \odot (1 - m), \quad (9)$$

and the process is repeated. In the final step, the entire region outside the mask is replaced with the corresponding region from the input image, thus strictly preserving the background. This straightforward but effective method for implementing foreground-background fusion is free from training diffusion architectures based on Inpainting.

## 4. Experiments

### 4.1. Datasets

To comprehensively evaluate the performance of various material transfer methods, we have established a freely available open-source dataset Material Transfer Benchmark (MTB) specifically designed to assess the efficacy of material transfer techniques. This dataset comprises 60 material images and 30 photographs of target objects as inputs.

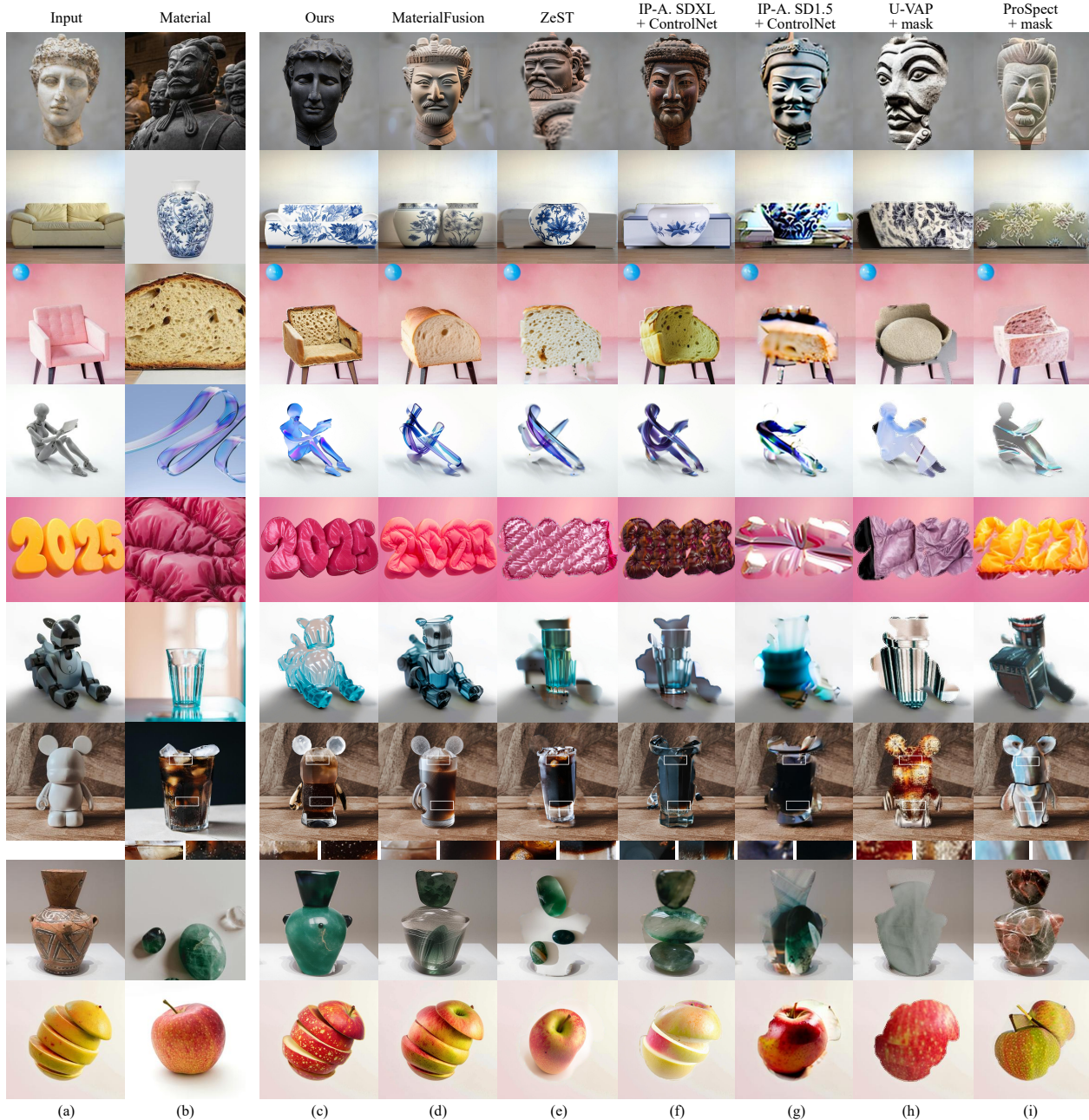


Figure 4. Qualitative comparison on the MTB dataset. MaTe demonstrates a distinct advantage in handling complex materials. (d)-(g) are based on work utilizing IP-Adapter and ControlNet, while (h) and (i) are based on fine-tuning with input images and texts.

All photos are from Unsplash [19], a website known for its copyright-free content, ensuring the dataset’s accessibility and usability for research purposes. Examples of the dataset are provided in the Supplementary Materials for reference.

## 4.2. Implementation Details

We build our method upon FLUX.1 [21], a latent rectified flow transformer for image generation. For our experiments, we set inference steps to 8 and configured the image generation size to  $1024 \times 1024$  pixels. Additionally, we uti-

lized a classifier-free guidance scale of 30. All experiments were conducted on a single NVIDIA A100 GPU.

For comparison experiments settings, we compare MaTe with MaterialFusion [9], ZeST [3], IP-Adapter SDXL [43], IP-Adapter SD1.5 [43], U-VAP [42], and ProSpect [49] in the task of material transfer. To enhance the fairness of the experiments, we added the corresponding version of the ControlNet depth control models [6, 46] to the pipelines for IP-Adapter SD1.5 and IP-Adapter SDXL. Additionally, we incorporated mask segmentation operations for IP-

|                       | Generation Quality |                    |                 | User Study         |                      |                    | Base model  | Preprocessing time (s) | Inference time (s) | Fine-tuning | Text conditions | Reference Networks |
|-----------------------|--------------------|--------------------|-----------------|--------------------|----------------------|--------------------|-------------|------------------------|--------------------|-------------|-----------------|--------------------|
|                       | SSIM $\uparrow$    | LPIPS $\downarrow$ | CLIP $\uparrow$ | Texture $\uparrow$ | Structure $\uparrow$ | Overall $\uparrow$ |             |                        |                    |             |                 |                    |
| ProSpect [49]         | 0.8048             | 0.1693             | 0.8009          | 2.57%              | 2.57%                | 1.84%              | SD1.4 [36]  | 200                    | 16                 | ✓           | ✓               | -                  |
| U-VAP [42]            | 0.7176             | 0.2612             | 0.7698          | 0.37%              | 0.18%                | 0.00%              | SD1.5 [36]  | 522                    | 7                  | ✓           | ✓               | -                  |
| IP-Adapter SD1.5 [43] | 0.7489             | 0.2537             | 0.8271          | 0.74%              | 0.37%                | 0.00%              | SD1.5 [36]  | 0                      | 10                 | -           | -               | ✓                  |
| IP-Adapter SDXL [43]  | 0.8152             | 0.1876             | 0.8358          | 7.35%              | 2.94%                | 3.49%              | SDXL [32]   | 0                      | 20                 | -           | -               | ✓                  |
| ZeST [3]              | 0.7231             | 0.2430             | <u>0.8627</u>   | 14.34%             | 0.18%                | 0.37%              | SDXL [32]   | 0                      | 21                 | -           | -               | ✓                  |
| MaterialFusion [9]    | <u>0.8263</u>      | <u>0.1565</u>      | 0.8521          | 11.21%             | 20.04%               | 10.48%             | SD1.5 [36]  | 0                      | 43                 | -           | ✓               | ✓                  |
| MaTe(Ours)            | <b>0.8617</b>      | <b>0.1319</b>      | <b>0.8825</b>   | 63.42%             | 73.71%               | 83.82%             | Flux.1 [21] | 0                      | 11                 | -           | -               | -                  |

Table 1. Quantitative comparisons with other methods are presented. MaTe and baselines are compared across common quantitative metrics, user studies, and model efficiency. The results that represent the current SOTA baselines for material transfer are highlighted in gray, with the best results shown in bold and the second-best results underlined.

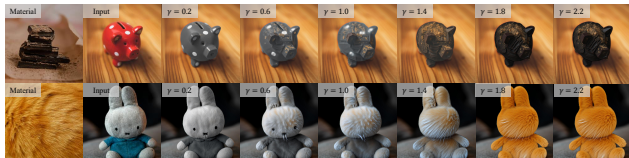


Figure 5. Material image effect intensity ablation experiment.

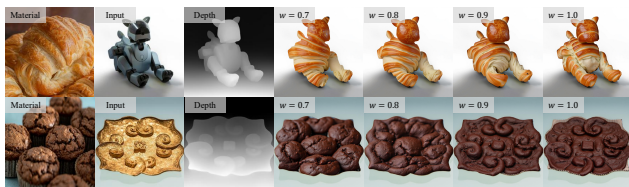


Figure 6. Ablation experiment on the depth control parameter  $w$ .

Adapters, U-VAP, and ProSpect.

### 4.3. Qualitative Comparison

As shown in Fig. 4, our method faithfully retains the structure of the input images. Material transfer based solely on image conditions is not possible with previous methods. MaTe ingeniously transfers appearance from the material image, capturing the correspondence between the subject and the material, achieving a balanced alignment of structural preservation and material representation. In contrast, personalized methods based on image fine-tuning [42, 49] did not show significant material transfer effects. Additionally, methods based on ControlNet + IP-Adapter [3, 9, 43, 47] (Fig. 4 (d)-(g)) often fail to maintain structure or transfer the appearance of the material. The latest state-of-the-art method, MaterialFusion, also struggles to balance the expression of structure and material information.

Specifically, in the chair case, we accurately captured the hollow structural features of the chair, which other methods failed to retain. In the composite material ribbon example, we restored material properties such as color gradient, transparency, and gloss. Furthermore, in the cola ice cube case, MaTe maintained the shape and spatial layout, which other methods failed to preserve. In the apple example, although the material image did not show the inner flesh, our method still accurately presented the apple’s material characteristics, to some extent indicating that the model aligned the material information and expressed a certain level of

prior understanding, while other methods had deviations in texture details, demonstrating the accuracy of our method in material understanding and transfer.

### 4.4. Quantitative Comparison

**Effect Comparison.** We conduct quantitative evaluations and comparisons with state-of-the-art material transfer methods on the MTB dataset. We use the Structural Similarity Index (SSIM) [41] to measure the structural consistency between the input images and the results, the Learned Perceptual Image Patch Similarity (LPIPS) [48] to assess the content detail consistency between the input images and the results, and the Contrastive Language–Image Pre-training (CLIP) [33] to evaluate the similarity between the materials and the results. The results are shown in Table 1. Our method outperforms all other methods across all metrics, demonstrating the effectiveness of our model architecture for the material transfer task.

**User Study.** The human subjective evaluation is divided into three parts: texture, structure, and overall results. We asked users to select their favorite outcome from all methods in each aspect. We sought a total of 16 evaluators who have experience in the vision and graphics field. Based on 34 sets of comparative results (each set includes 7 methods), evaluations were conducted from three perspectives, yielding 1,632 voting results. The percentages in columns 5 – 7 of Table 1 reflect the voting situation of the users, indicating that the results generated by our proposed MaTe are more favored in all three aspects. We note the difference between objective and subjective evaluation metrics: while objective metrics assess aspects in isolation, users may integrate information across aspects despite being provided with separate options. Human preference implies that our generated outcomes have struck a better balance among texture, structure, and overall visual appeal. For detailed information, please refer to the Supplementary Materials.

**Efficiency comparison.** Column 8 of Table 1 lists the diffusion model versions used by different methods, among which we use Flux.1 as the basic model, highlighting the innovation and advancement of MaTe. Columns 9-10 further compare preprocessing time and inference time. By eliminating ControlNet or additional text or image encoders,



Figure 7. Regarding the ablation experiment results when  $C_I$  is set to different images.



Figure 8. The visualization results when CFG changes linearly.

our framework achieves significant time reduction throughout the inference process. Finally, columns 11-13 illustrate MaTe is the first method that does not require fine-tuning, text, or reference networks, demonstrating its user-friendliness and practicality.

#### 4.5. Ablation Studies

We conduct ablation experiments to study the effects of varying 1) material image influence strength, 2) depth image influence strength, 3) optical restoration, and 4) classification guidance (CFG) influence strength. As illustrated in Figure 5, when the Cross-Bias strength factor  $\gamma$  approaches 0, the material information exerts minimal influence. A satisfactory material transfer effect is achieved as  $\gamma$  increases to 1.8. However, further increments of  $\gamma$  beyond this value lead to diminishing returns, with little additional improvement observed. Fig. 6 illustrates the outcomes of controlling depth with different strengths of LoRA influence, where  $w$  takes values in  $\{0.7, 0.8, 0.9, 1.0\}$ . The results demonstrate that  $w$  can effectively control the influence of depth information, thus allowing for flexible control over its impact. Furthermore, to validate the effectiveness of illumination image restoration for input image lighting, we compare the generated results with those using the original image and random noise as inputs. As shown in Fig. 7, the original input image significantly interferes with the color of the production results, while random noise completely disregards the lighting information of the input image, causing the lighting results to lean more towards the material image. Lastly, we run inferences with CFG strengths of  $\{10, 20, 30, 40, 50\}$ . Fig. 8 shows that increasing CFG strength enhances image detail and fidelity. However, beyond a certain threshold, color distortion and high-frequency noise appear. In our experiments, we consistently use a CFG strength of 30, which we find to be optimal for our purposes.

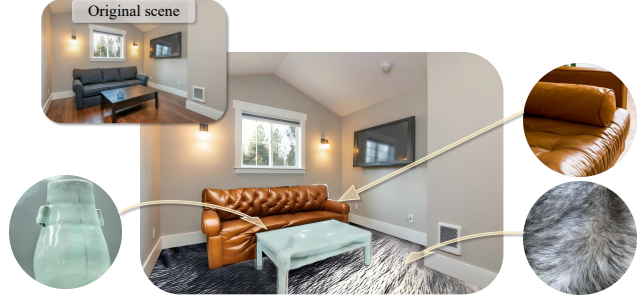


Figure 9. Multi-object material transfer in the real-world scene.

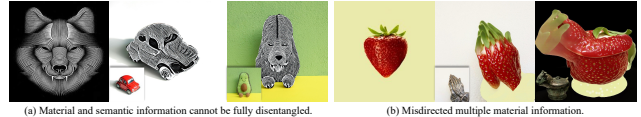


Figure 10. Limitations. When the semantic information in the material image is too entangled with the texture information, MaTe may struggle to transfer only the texture information.

#### 4.6. Applications

By replacing the foreground extraction with a segmentation module (such as SAM [34, 50]) to obtain multiple masks, a variety of materials can be applied to multiple objects. Fig. 9 demonstrates that MaTe can edit multiple objects within a single image, as illustrated by the material editing performed on the sofa, table, and floors in the image, showcasing MaTe's robustness and its applicability to editing complex real-world scenarios.

#### 4.7. Limitations

Based on our observations, MaTe currently has two main limitations: 1) If the material is closely entangled with its semantic information, some of the semantic information may also be transferred to the target object. For instance, in Fig. 10 (a), the wolf information from the line art is transferred onto an avocado. 2) Since there are no restrictions on the input material images, it is possible that multiple material information from the materials may be transferred. For example, in Fig. 10 (b), the yellow background of the material image is transferred to the result.

### 5. Conclusion

In this paper, we present MaTe, a streamlined and efficient diffusion model for material transfer that operates without additional training or fine-tuning. By enabling semantic alignment and information mining across illumination, material, and depth images, MaTe achieves material transfer from arbitrary 2D images to target objects while simplifying the inference workflow. Extensive experiments demonstrate that MaTe yields state-of-the-art qualitative and quantitative performance, surpassing existing methods while maintaining a compact and computationally efficient architecture.

## 6. Acknowledgment

The work is supported in part by the Science and Technology Innovation 2030 – major project brain-inspired learning and game theory for non-cooperative heterogeneous multi-agent systems, China, under Project No. 2021ZD0201404, and the National Science and Technology Council, Taiwan, under Project No. 113-2221-E-006-161-MY3.

## References

- [1] Dave Zhenyu Chen, Yawar Siddiqui, Hsin-Ying Lee, Sergey Tulyakov, and Matthias Nießner. Text2tex: Text-driven texture synthesis via diffusion models. In *Proceedings of the IEEE/CVF International Conference on Computer Vision*, pages 18558–18568, 2023. 3
- [2] Junsong Chen, YU Jincheng, GE Chongjian, Lewei Yao, Enze Xie, Zhongdao Wang, James Kwok, Ping Luo, Huchuan Lu, and Zhenguo Li. Pixart- $\alpha$ : Fast training of diffusion transformer for photorealistic text-to-image synthesis. In *The Twelfth International Conference on Learning Representations*. 3
- [3] Ta-Ying Cheng, Prafull Sharma, Andrew Markham, Niki Trigoni, and Varun Jampani. Zest: Zero-shot material transfer from a single image. In *European Conference on Computer Vision*, pages 370–386. Springer, 2024. 2, 3, 4, 6, 7
- [4] Zheng Chong, Xiao Dong, Haoxiang Li, Wenqing Zhang, Hanqing Zhao, Dongmei Jiang, Xiaodan Liang, et al. Catvton: Concatenation is all you need for virtual try-on with diffusion models. In *The Thirteenth International Conference on Learning Representations*. 2
- [5] Valentin Deschaintre, Miika Aittala, Fredo Durand, George Drettakis, and Adrien Bousseau. Single-image svbrdf capture with a rendering-aware deep network. *ACM Transactions on Graphics (ToG)*, 37(4):1–15, 2018. 1
- [6] Diffusers. controlnet-depth-sdxl-1.0. <https://huggingface.co/diffusers/controlnet-depth-sdxl-1.0.6>
- [7] Patrick Esser, Sumith Kulal, Andreas Blattmann, Rahim Entezari, Jonas Müller, Harry Saini, Yam Levi, Dominik Lorenz, Axel Sauer, Frederic Boesel, et al. Scaling rectified flow transformers for high-resolution image synthesis. In *International Conference on Machine Learning*, pages 12606–12633. PMLR, 2024. 2, 3
- [8] Rinon Gal, Yuval Alaluf, Yuval Atzmon, Or Patashnik, Amit Haim Bermano, Gal Chechik, and Daniel Cohen-or. An image is worth one word: Personalizing text-to-image generation using textual inversion. In *The Eleventh International Conference on Learning Representations*. 2
- [9] Kamil Garifullin, Maxim Nikolaev, Andrey Kuznetsov, and Aibek Alanov. Materialfusion: High-quality, zero-shot, and controllable material transfer with diffusion models. *arXiv preprint arXiv:2502.06606*, 2025. 2, 3, 4, 6, 7
- [10] Philipp Henzler, Valentin Deschaintre, Niloy J Mitra, and Tobias Ritschel. Generative modelling of brdf textures from flash images. *ACM Transactions on Graphics (ToG)*, 40(6):1–13, 2021. 1
- [11] Amir Hertz, Ron Mokady, Jay Tenenbaum, Kfir Aberman, Yael Pritch, and Daniel Cohen-or. Prompt-to-prompt image editing with cross-attention control. In *The Eleventh International Conference on Learning Representations*. 2
- [12] Edward J Hu, Phillip Wallis, Zeyuan Allen-Zhu, Yuanzhi Li, Shean Wang, Lu Wang, Weizhu Chen, et al. Lora: Low-rank adaptation of large language models. In *The Tenth International Conference on Learning Representations*. 2, 4
- [13] Yiwei Hu, Julie Dorsey, and Holly Rushmeier. A novel framework for inverse procedural texture modeling. *ACM Transactions on Graphics (ToG)*, 38(6):1–14, 2019. 1
- [14] Yiwei Hu, Chengan He, Valentin Deschaintre, Julie Dorsey, and Holly Rushmeier. An inverse procedural modeling pipeline for svbrdf maps. *ACM Transactions on Graphics (ToG)*, 41(2):1–17, 2022. 1
- [15] Nisha Huang, Fan Tang, Weiming Dong, and Changsheng Xu. Draw your art dream: Diverse digital art synthesis with multimodal guided diffusion. In *Proceedings of the 30th ACM International Conference on Multimedia*, pages 1085–1094, 2022. 2
- [16] Nisha Huang, Yuxin Zhang, Fan Tang, Chongyang Ma, Haibin Huang, Weiming Dong, and Changsheng Xu. Diffstyler: Controllable dual diffusion for text-driven image stylization. *IEEE Transactions on Neural Networks and Learning Systems*, 2024. 2
- [17] Nisha Huang, Weiming Dong, Yuxin Zhang, Fan Tang, Ronghui Li, Chongyang Ma, Xiu Li, Tong-Yee Lee, and Changsheng Xu. Creativesynth: Cross-art-attention for artistic image synthesis with multimodal diffusion. *IEEE Transactions on Visualization and Computer Graphics*, 2025. 2
- [18] Nisha Huang, Kaer Huang, Yifan Pu, Jiangshan Wang, Jie Guo, Yiqiang Yan, Xiu Li, and Tong-Yee Lee. Artcrafter: Text-image aligning style transfer via embedding reframing. *arXiv preprint arXiv:2501.02064*, 2025. 2
- [19] Unsplash Inc. Unsplash. <https://unsplash.com/>. 6
- [20] Diederik P. Kingma and Max Welling. Auto-encoding variational bayes. In *The Second International Conference on Learning Representations*. 4
- [21] Black Forest Labs. Flux. <https://github.com/black-forest-labs/flux>, . 3, 6, 7
- [22] Black Forest Labs. Flux.1-depth-dev-lora. <https://huggingface.co/black-forest-labs/FLUX.1-Depth-dev-lora>, . 5
- [23] Black Forest Labs. Flux.1-dev-controlnet-depth. <https://huggingface.co/Shakker-Labs/FLUX.1-dev-ControlNet-Depth>, . 4
- [24] Kuan Heng Lin, Sicheng Mo, Ben Klingher, Fangzhou Mu, and Bolei Zhou. Ctrl-x: Controlling structure and appearance for text-to-image generation without guidance. In *Advances in Neural Information Processing Systems*, 2024. 2
- [25] Yaron Lipman, Ricky TQ Chen, Heli Ben-Hamu, Maximilian Nickel, and Matthew Le. Flow matching for generative modeling. In *The Eleventh International Conference on Learning Representations*. 3
- [26] Xingchao Liu, Chengyue Gong, et al. Flow straight and fast: Learning to generate and transfer data with rectified flow. In *The Eleventh International Conference on Learning Representations*. 3

- [27] Ivan Lopes, Fabio Pizzati, and Raoul de Charette. Material palette: extraction of materials from a single image. In *Proceedings of the IEEE/CVF Conference on Computer Vision and Pattern Recognition*, pages 4379–4388, 2024. 2, 3
- [28] Pengqi Lu. Qwen2vl-flux: Unifying image and text guidance for controllable image generation, 2024. 2
- [29] Chong Mou, Xintao Wang, Liangbin Xie, Yanze Wu, Jian Zhang, Zhongang Qi, and Ying Shan. T2i-adapter: Learning adapters to dig out more controllable ability for text-to-image diffusion models. In *Proceedings of the AAAI conference on artificial intelligence*, pages 4296–4304, 2024. 3, 5
- [30] Zexu Pan, Zhaojie Luo, Jichen Yang, and Haizhou Li. Multimodal attention for speech emotion recognition. In *Proc. Interspeech 2020*, pages 364–368, 2020. 3
- [31] William Peebles and Saining Xie. Scalable diffusion models with transformers. In *Proceedings of the IEEE/CVF International Conference on Computer Vision*, pages 4195–4205, 2023. 2, 3
- [32] Dustin Podell, Zion English, Kyle Lacey, Andreas Blattmann, Tim Dockhorn, Jonas Müller, Joe Penna, and Robin Rombach. Sdxl: Improving latent diffusion models for high-resolution image synthesis. In *The Twelfth International Conference on Learning Representations*. 7
- [33] Alec Radford, Jong Wook Kim, Chris Hallacy, Aditya Ramesh, Gabriel Goh, Sandhini Agarwal, Girish Sastry, Amanda Askell, Pamela Mishkin, Jack Clark, et al. Learning transferable visual models from natural language supervision. In *International Conference on Machine Learning*, pages 8748–8763. PMLR, 2021. 7
- [34] Nikhila Ravi, Valentin Gabeur, Yuan-Ting Hu, Ronghang Hu, Chaitanya Ryali, Tengyu Ma, Haitham Khedr, Roman Rädle, Chloe Rolland, Laura Gustafson, Eric Mintun, Junting Pan, Kalyan Vasudev Alwala, Nicolas Carion, Chao-Yuan Wu, Ross Girshick, Piotr Dollár, and Christoph Feichtenhofer. Sam 2: Segment anything in images and videos. *arXiv preprint arXiv:2408.00714*, 2024. 8
- [35] Elad Richardson, Gal Metzer, Yuval Alaluf, Raja Giryes, and Daniel Cohen-Or. Texture: Text-guided texturing of 3d shapes. In *ACM SIGGRAPH 2023 Conference Proceedings*, pages 1–11, 2023. 3
- [36] Robin Rombach, Andreas Blattmann, Dominik Lorenz, Patrick Esser, and Björn Ommer. High-resolution image synthesis with latent diffusion models. In *Proceedings of the IEEE/CVF Conference on Computer Vision and Pattern Recognition*, pages 10684–10695, 2022. 2, 4, 7
- [37] Nataniel Ruiz, Yuanzhen Li, Varun Jampani, Yael Pritch, Michael Rubinstein, and Kfir Aberman. Dreambooth: Fine tuning text-to-image diffusion models for subject-driven generation. In *Proceedings of the IEEE/CVF Conference on Computer Vision and Pattern Recognition*, pages 22500–22510, 2023. 2, 3
- [38] Prafull Sharma, Varun Jampani, Yuanzhen Li, Xuhui Jia, Dmitry Lagun, Fredo Durand, Bill Freeman, and Mark Matthews. Alchemist: Parametric control of material properties with diffusion models. In *Proceedings of the IEEE/CVF Conference on Computer Vision and Pattern Recognition*, pages 24130–24141, 2024. 2
- [39] Jiaming Song, Chenlin Meng, and Stefano Ermon. Denoising diffusion implicit models. In *International Conference on Learning Representations*. 3
- [40] Jianlin Su, Murtadha Ahmed, Yu Lu, Shengfeng Pan, Wen Bo, and Yunfeng Liu. Roformer: Enhanced transformer with rotary position embedding. *Neurocomputing*, 568:127063, 2024. 3
- [41] Zhou Wang, Alan C Bovik, Hamid R Sheikh, and Eero P Simoncelli. Image quality assessment: from error visibility to structural similarity. *IEEE Transactions on Image Processing*, 13(4):600–612, 2004. 7
- [42] You Wu, Kean Liu, Xiaoyue Mi, Fan Tang, Juan Cao, and Jintao Li. U-vap: User-specified visual appearance personalization via decoupled self augmentation. In *Proceedings of the IEEE/CVF Conference on Computer Vision and Pattern Recognition*, pages 9482–9491, 2024. 2, 3, 6, 7
- [43] Hu Ye, Jun Zhang, Sibio Liu, Xiao Han, and Wei Yang. Ip-adapter: Text compatible image prompt adapter for text-to-image diffusion models. *arXiv preprint arxiv:2308.06721*, 2023. 2, 3, 4, 6, 7
- [44] Chih-Kuo Yeh, Zhanping Liu, I-Hsuan Lin, Eugene Zhang, and Tong-Yee Lee. Wysiwyg design of hypnotic line art. *IEEE Transactions on Visualization and Computer Graphics*, 28(6):2517–2529, 2020. 1
- [45] Yu-Ying Yeh, Jia-Bin Huang, Changil Kim, Lei Xiao, Thu Nguyen-Phuoc, Numair Khan, Cheng Zhang, Manmohan Chandraker, Carl S Marshall, Zhao Dong, et al. Texture-dreamer: Image-guided texture synthesis through geometry-aware diffusion. In *Proceedings of the IEEE/CVF Conference on Computer Vision and Pattern Recognition*, pages 4304–4314, 2024. 3
- [46] Lvmin Zhang. Controlnet-v1.1-depth. [https://huggingface.co/lllyasviel/control\\_v11f1p\\_sd15\\_depth](https://huggingface.co/lllyasviel/control_v11f1p_sd15_depth). 6
- [47] Lvmin Zhang, Anyi Rao, and Maneesh Agrawala. Adding conditional control to text-to-image diffusion models. In *Proceedings of the IEEE/CVF International Conference on Computer Vision*, pages 3836–3847, 2023. 2, 3, 5, 7
- [48] Richard Zhang, Phillip Isola, Alexei A Efros, Eli Shechtman, and Oliver Wang. The unreasonable effectiveness of deep features as a perceptual metric. In *Proceedings of the IEEE Conference on Computer Vision and Pattern Recognition*, pages 586–595, 2018. 7
- [49] Yuxin Zhang, Weiming Dong, Fan Tang, Nisha Huang, Haibin Huang, Chongyang Ma, Tong-Yee Lee, Oliver Deussen, and Changsheng Xu. Prospect: Prompt spectrum for attribute-aware personalization of diffusion models. *ACM Transactions on Graphics (ToG)*, 42(6):1–14, 2023. 2, 3, 6, 7
- [50] Yuxuan Zhang, Tianheng Cheng, Rui Hu, Lei Liu, Heng Liu, Longjin Ran, Xiaoxin Chen, Wenyu Liu, and Xing-gang Wang. Evf-sam: Early vision-language fusion for text-prompted segment anything model. 2024. 8